Weierstraß–Institut
für Angewandte Analysis und Stochastik

im Forschungsverbund Berlin e.V.

On time counting procedures in the DSMC method for rarefied gases

Sergej Rjasanow[1] , Wolfgang Wagner[2]

submitted: 29 July 1997

[1] University of Saarbrücken
Department of Mathematics
PF 15 11 50
D – 66041 Saarbrücken
Germany
eMail: rjasanow@num.uni-sb.de

[2] Weierstrass Institute
for Applied Analysis
and Stochastics
Mohrenstraße 39
D – 10117 Berlin
Germany
eMail: wagner@wias-berlin.de

Preprint No. 349
Berlin 1997

1991 Mathematics Subject Classification. 65C05, 76P05, 82C80.

Key words and phrases. DSMC method, rarefied gas dynamics, Boltzmann equation, time counting procedures, numerical experiments.

Edited by
Weierstraß–Institut für Angewandte Analysis und Stochastik (WIAS)
Mohrenstraße 39
D — 10117 Berlin
Germany

Fax: + 49 30 2044975
e–mail (X.400): c=de;a=d400-gw;p=WIAS-BERLIN;s=preprint
e–mail (Internet): preprint@wias-berlin.de
World Wide Web: http://www.wias-berlin.de/

Abstract. The DSMC (direct simulation Monte Carlo) method for rarefied gas dynamics is studied. The behaviour of the underlying stochastic particle system is determined by three main components - the time step between subsequent collisions, the random mechanism for the choice of the collision partners, and the random mechanism for calculating the result of the collision. The purpose of this paper is to illustrate the interplay between these various components and to propose some new modifications of the DSMC method. Different time counting procedures are derived and their influence on the other parts of the algorithm is investigated. Various modifications of the DSMC method are compared with respect to different criteria such as efficiency, systematic error, and statistical fluctuations.

Contents

1. Introduction

A commonly used tool for the numerical treatment of rarefied gas flows in real world applications (like the reentry of a space shuttle into the atmosphere) is the DSMC (direct simulation Monte Carlo) method (see, e.g., [9]). This method had been developed by G. A. Bird since the sixties (cf. [1], [2], [3]).

An important part of the DSMC method is the mechanism that determines the number of collisions among the simulation particles during a given time interval. The original procedure, called "time counter", assigned an appropriate individual amount of time to each of the collisions. Later this procedure was replaced by a tool that was called "no time counter" method, so as to be clearly distinguished from the previous one. Here the number of collisions on the given time interval was calculated in advance, which is numerically more convenient. We refer to [8], [4] and the detailed discussion of this development in [5, § 11.1].

From a mathematical point of view, the time evolution of rarefied gas flows is described by the Boltzmann equation (see, e.g., [6], [7]). The relationship between the DSMC method and the Boltzmann equation was established in [11], where both the "time counter" and the "no time counter" versions of the method were treated. Stochastic interacting particle systems and, in particular, Markov jump processes, turned out to be a convenient mathematical model for the description and unification of different numerical procedures in rarefied gas dynamics. We refer to [7, Ch. 10], [12], [10] for more details and references related to particle methods for the Boltzmann equation.

Generally speaking, the behaviour of the stochastic particle system is determined by three main components - the time step between subsequent interactions (collisions), the random mechanism for the choice of the collision partners, and the (again random) mechanism for calculating the result of the collision. The **purpose of this paper** is to illustrate the interplay between these various components and to propose some new modifications of the DSMC method.

Section 2 contains some material about stochastic processes related to rarefied gas dynamics, which we need for the presentation of the subject. The main results are contained in Section 3. Here we derive different time counting procedures and show how they influence the other (random) parts of the corresponding algorithms. Section 4 contains the results of numerical experiments. Here we compare the various modifications of the DSMC method with respect to different criteria such as efficiency, systematic error, and statistical fluctuations.

2. Preliminaries

2.1. The Boltzmann equation

The Boltzmann equation for dilute monatomic gases ([6]) takes the form

$$\frac{\partial}{\partial t} f(t,x,v) + (v, \nabla_x) f(t,x,v) = \tag{2.1}$$
$$\int_{\mathcal{R}^3} dw \int_{\mathcal{S}^2} de\, B(v,w,e) \left[f(t,x,v^*) f(t,x,w^*) - f(t,x,v) f(t,x,w) \right],$$

where $t \geq 0$, $x \in D \subset \mathcal{R}^3$, $v \in \mathcal{R}^3$, and appropriate initial and boundary conditions are assumed. The symbol ∇_x denotes the vector of the partial derivatives with respect to x, D is a bounded domain in the three–dimensional Euclidean space $\mathcal{R}^3$, and $(.,.)$ is the scalar product. The function B is called the collision kernel. The symbols de and dw denote the uniform surface measure on the unit sphere $\mathcal{S}^2$ and the Lebesgue measure on $\mathcal{R}^3$, respectively. The objects v^* and w^* are defined as

$$v^* = v + e\,(e, w - v)\,, \quad w^* = w + e\,(e, v - w)\,,$$

where $v, w \in \mathcal{R}^3$, $e \in \mathcal{S}^2$. They are interpreted as the post–collision velocities of two particles with the pre–collision velocities v and w.

Various approximations involved in the DSMC algorithm are related to some approximations of the Boltzmann equation (2.1). First there is a splitting of the free flow simulation and the collision simulation on a small time interval. Second a partition

$$D = \cup_{l=1}^{l_c} D_l \tag{2.2}$$

of the spatial domain D into a finite number l_c of disjoint cells is used during the collision simulation step. Thus, the limiting equation (as the number of simulation particles tends to infinity) corresponding to the collision simulation step of the DSMC algorithm has the form (cf. [11])

$$\frac{\partial}{\partial t} f(t,x,v) = \tag{2.3}$$
$$\int_D dy \int_{\mathcal{R}^3} dw \int_{\mathcal{S}^2} de\, h(x,y)\, B(v,w,e)\Big[f(t,x,v^*)\, f(t,y,w^*) - f(t,x,v)\, f(t,y,w)\Big].$$

The function

$$h(x,y) = \sum_{l=1}^{l_c} \frac{1}{|D_l|} \P_{D_l}(x)\, \P_{D_l}(y)\,, \tag{2.4}$$

is a mollifying kernel depending on the partition (2.2), where $|D_l|$ is the Lebesgue measure of the cell D_l, and $\P$ denotes the indicator function.

2.2. The basic Markov process

The stochastic process related to the mollified Boltzmann equation (2.3) has the infinitesimal generator

$$\mathcal{A}(\Phi)(\bar{z}) = \frac{1}{2} \sum_{1 \leq i \neq j \leq n} \int_{\mathcal{S}^2} q(z_i, z_j, e)\Big[\Phi(J(\bar{z}, i, j, e)) - \Phi(\bar{z})\Big]\, de\,, \tag{2.5}$$

where

$$\bar{z} = (z_1, \ldots, z_n) = ((x_1, v_1), \ldots, (x_n, v_n)) \tag{2.6}$$

and

$$[J(\bar{z}, i, j, e)]_k = \begin{cases} (x_k, v_k)\,, \text{ if } & k \neq i, j\,, \\ (x_i, v_i^*)\,, \text{ if } & k = i\,, \\ (x_j, v_j^*)\,, \text{ if } & k = j\,. \end{cases}$$

The function q will be specified later.

The generator (2.5) can be rewritten in the usual form of a jump process generator

$$\mathcal{A}(\Phi)(\bar{z}) = \int_{\mathcal{Z}} \left[\Phi(\bar{\zeta}) - \Phi(\bar{z})\right] \mathcal{Q}(\bar{z}, d\bar{\zeta}), \tag{2.7}$$

where

$$\mathcal{Q}(\bar{z}, d\bar{\zeta}) = \frac{1}{2} \sum_{1 \le i \ne j \le n} \int_{\mathcal{S}^2} \delta_{J(\bar{z},i,j,e)}(d\bar{\zeta})\, q(z_i, z_j, e)\, de$$

and δ denotes the Dirac measure. The generator (2.7) does not change if one replaces $\mathcal{Q}$ by

$$\hat{\mathcal{Q}}(\bar{z}, d\bar{\zeta}) = \tag{2.8}$$
$$\frac{1}{2} \sum_{1 \le i \ne j \le n} \left\{ \int_{\mathcal{S}^2} \delta_{J(\bar{z},i,j,e)}(d\bar{\zeta})\, q(z_i, z_j, e)\, de + \delta_{\bar{z}}(d\bar{\zeta}) \left[\hat{q}(z_i, z_j) - \int_{\mathcal{S}^2} q(z_i, z_j, e)\, de\right] \right\},$$

where $\hat{q}$ is a function such that

$$\int_{\mathcal{S}^2} q(z_i, z_j, e)\, de \le \hat{q}(z_i, z_j). \tag{2.9}$$

Remark 2.1 *Note that the distribution of the process does not depend on the function $\hat{q}$. However, the choice of this function provides different ways of generating trajectories of the process.*

The behaviour of the Markov process with the infinitesimal generator (2.7), (2.8) is described as follows.

Coming to a state $\bar{z}$ (cf. (2.6)), the process stays there for a **random waiting time** $\hat{\tau}(\bar{z})$, which has an exponential distribution with the parameter

$$\hat{\pi}(\bar{z}) = \hat{\mathcal{Q}}(\bar{z}, \mathcal{Z}) = \frac{1}{2} \sum_{1 \le i \ne j \le n} \hat{q}(z_i, z_j), \tag{2.10}$$

i.e.

$$\mathrm{Prob}\left\{\hat{\tau}(\bar{z}) \ge t\right\} = \exp(-\hat{\pi}(\bar{z})\, t).$$

Note that the expectation of the random waiting time is

$$\hat{\pi}(\bar{z})^{-1}.$$

If this value is sufficiently small, it can be used as a deterministic approximation to the random time step $\hat{\tau}(\bar{z})$.

Then the process jumps into a state $\bar{\zeta}$, which is distributed according to the **jump distribution**

$$\hat{\pi}(\bar{z})^{-1}\, \hat{\mathcal{Q}}(\bar{z}, d\bar{\zeta}).$$

This distribution represents a superposition of simpler distributions (cf. (2.8)),

$$\hat{\pi}(\bar{z})^{-1}\,\hat{Q}(\bar{z},d\bar{\zeta}) = \sum_{1\le i\ne j\le n} \frac{\hat{q}(z_i,z_j)}{2\,\hat{\pi}(\bar{z})} \left\{ \frac{\int_{S^2} q(z_i,z_j,e)\,de}{\hat{q}(z_i,z_j)} \int_{S^2} \delta_{J(\bar{z},i,j,e)}(d\bar{\zeta})\, \frac{q(z_i,z_j,e)}{\int_{S^2} q(z_i,z_j,e)\,de}\,de + \delta_{\bar{z}}(d\bar{\zeta}) \left[1 - \frac{\int_{S^2} q(z_i,z_j,e)\,de}{\hat{q}(z_i,z_j)} \right] \right\}.$$

Consequently, first the **distribution of the parameters i and j** is determined by the probabilities

$$\frac{\hat{q}(z_i,z_j)}{2\,\hat{\pi}(\bar{z})} = \frac{\hat{q}(z_i,z_j)}{\sum_{1\le i\ne j\le n} \hat{q}(z_i,z_j)}\,. \tag{2.11}$$

Given i and j, there is a certain **probability that the jump is fictitious**. Namely, the new state is $\bar{\zeta} = \bar{z}$ with probability

$$1 - \frac{\int_{S^2} q(z_i,z_j,e)\,de}{\hat{q}(z_i,z_j)}\,. \tag{2.12}$$

Otherwise, the **distribution of the parameter e** is

$$\frac{q(z_i,z_j,e)}{\int_{S^2} q(z_i,z_j,e)\,de}\,, \tag{2.13}$$

and the new state is $\bar{\zeta} = J(\bar{z},i,j,e)$.

2.3. Modelling of the cell process

The stochastic process related to the collision simulation step in one spatial cell D_l (cf. (2.3), (2.4)) corresponds to the function (cf. (2.5))

$$q(z_i,z_j,e) = \frac{1}{n}\,\frac{1}{|D_l|}\,\P_{D_l}(x_i)\,\P_{D_l}(x_j)\,B(v_i,v_j,e)\,.$$

We choose

$$\hat{q}(z_i,z_j) = \frac{1}{n}\,\frac{1}{|D_l|}\,\P_{D_l}(x_i)\,\P_{D_l}(x_j)\,\hat{B}(v_i,v_j)\,, \tag{2.14}$$

where

$$\int_{S^2} B(v_i,v_j,e)\,de \le \hat{B}(v_i,v_j)\,, \tag{2.15}$$

so that condition (2.9) is satisfied.

We specify the general modelling procedure from the previous section according to (2.14). The parameter (2.10) of the waiting time distribution takes the form

$$\hat{\pi}(\bar{z}) = \frac{1}{2\,n\,|D_l|} \sum_{i\ne j\,:\,x_i,x_j\in D_l} \hat{B}(v_i,v_j)\,. \tag{2.16}$$

The distribution (2.11) of i, j is concentrated on the set $\{i : x_i \in D_l\}$ and takes the form

$$\frac{\hat{B}(v_i, v_j)}{\sum_{i \neq j\,:\, x_i, x_j \in D_l} \hat{B}(v_i, v_j)}\,. \tag{2.17}$$

The probability (2.12) of a fictitious jump is

$$1 - \frac{\int_{S^2} B(v_i, v_j, e)\, de}{\hat{B}(v_i, v_j)}\,. \tag{2.18}$$

Finally, the distribution (2.13) of e is

$$\frac{B(v_i, v_j, e)}{\int_{S^2} B(v_i, v_j, e)\, de}\,. \tag{2.19}$$

2.4. Example: Hard sphere molecules

Consider the collision kernel B of the form

$$B(v_i, v_j, e) = \frac{c_B}{2\pi} \left|(v_i - v_j, e)\right|,$$

for some constant c_B. In this case, one obtains

$$\begin{aligned} \int_{S^2} B(v_i, v_j, e)\, de &= \frac{c_B}{2\pi} \int_0^{\pi} d\varphi_1 \int_0^{2\pi} d\varphi_2 \, \|v_i - v_j\| \, |\cos\varphi_1| \sin\varphi_1 \\ &= 2\, c_B \, \|v_i - v_j\| \int_0^{\pi/2} \cos\varphi_1 \, \sin\varphi_1 \, d\varphi_1 \\ &= 2\, c_B \, \|v_i - v_j\| \int_0^1 y \, dy = c_B \, \|v_i - v_j\|\,. \end{aligned} \tag{2.20}$$

Consequently, condition (2.15) takes the form

$$c_B \, \|v_i - v_j\| \leq \hat{B}(v_i, v_j)\,. \tag{2.21}$$

A trivial choice of the function $\hat{B}$ is

$$\hat{B}(v_i, v_j) = \int_{S^2} B(v_i, v_j, e)\, de = c_B \, \|v_i - v_j\|\,,$$

which gives the "original" behaviour of the process. In this case, the parameter (2.16) of the waiting time distribution takes the form

$$\hat{\pi}(\bar{z}) = \frac{c_B}{2n\,|D_l|} \sum_{i \neq j\,:\, x_i, x_j \in D_l} \|v_i - v_j\|\,. \tag{2.22}$$

The distribution (2.17) of i, j is

$$\frac{\|v_i - v_j\|}{\sum_{i \neq j\,:\, x_i, x_j \in D_l} \|v_i - v_j\|}\,, \tag{2.23}$$

i.e. the pairs of particles are chosen with probability proportional to their relative velocity. The probability (2.18) of a fictitious jump is zero. Finally, the distribution (2.19) of e is

$$\frac{\left|(v_i - v_j, e)\right|}{2\pi \, \|v_i - v_j\|}\,. \tag{2.24}$$

2.5. Statement of the problem

The modelling procedure for the stochastic particle system with the generator (2.5) is extremely simple. However, the numerical application may face serious problems if the number of particles n is large. In general, one has quadratic (with respect to n) effort in the calculation of the waiting time parameter (2.22) or the probabilities (2.23). Therefore, it is important to look for an appropriate choice of the function $\hat{B}$ in (2.15), which may lead to a substantial gain in the efficiency of the modelling of the process.

For an efficient numerical implementation, there are three points to be taken into account:

1. The inverse time step (2.16) should be easy to compute and not too big.
2. The distribution (2.17) of i, j should be easy to generate.
3. The probability (2.18) of fictitious jumps should be as small as possible.

3. Time counting procedures

3.1. The acceptance–rejection technique

The technique based on the following lemma is useful in many modifications of the DSMC method.

Lemma 3.1 *Consider a measurable space (X, μ) and two functions f and F on X satisfying the* **majorant condition**

$$0 \le f(x) \le F(x), \quad \forall x \in X .$$

Assume that

$$\int_X f(x)\,\mu(dx) > 0 \quad \textit{and} \quad \int_X F(x)\,\mu(dx) < \infty .$$

Let a random variable ξ be defined by the following procedure:

1. *Generate a random variable η with the probability density*

$$P(x) = \frac{F(x)}{\int_X F(x)\,\mu(dx)} . \tag{3.1}$$

2. *Generate independently a random variable u uniformly distributed on $[0,1]$.*
3. *If the* **acceptance condition**

$$u \le \frac{f(\eta)}{F(\eta)} \tag{3.2}$$

is satisfied, then $\xi = \eta$ and stop.

4. *If (3.2) is not fulfilled, then go to 1.*

Then the random variable ξ has the probability density

$$p(x) = \frac{f(x)}{\int_X f(x)\,\mu(dx)} . \tag{3.3}$$

Remark 3.2 *Lemma 3.1 shows how to model the density (3.3) on the basis of a modelling procedure for the density (3.1). Note that one does not need to know the normalizing constant* $\int_X f(x)\,\mu(dx)$.

3.2. Bird's time counter

First the indices i, j are generated according to the distribution (2.23). This is done with the acceptance–rejection technique. One considers the set

$$X = \{1 \le i \ne j \le n\}$$

and the functions

$$f_{i,j} = \|v_i - v_j\|\,, \qquad F_{i,j} = c\,,$$

where c is a constant satisfying

$$\|v_i - v_j\| \le c\,, \quad \forall i, j \in X\,.$$

Accordingly, the indices i, j are generated uniformly on X and accepted if (cf. (3.2))

$$u \le \frac{\|v_i - v_j\|}{c}\,.$$

The corresponding time step is then computed as (cf. (2.22))

$$\hat{\tau}(\bar{z}, i, j) = \left[\frac{c_B}{2n\,|D_l|}\,\|v_i - v_j\| \sum_{i \ne j\,:\,x_i, x_j \in D_l}\right]^{-1} = \frac{2n\,|D_l|}{c_B\,n_l\,(n_l - 1)\,\|v_i - v_j\|}\,, \tag{3.4}$$

where $n_l = n_l(\bar{z})$ denotes the number of particles in the cell D_l. Note that according to (2.23)

$$\begin{aligned} E\,\hat{\tau}(\bar{z}, i, j) &= \sum_{i \ne j\,:\,x_i, x_j \in D_l} \hat{\tau}(\bar{z}, i, j)\,\frac{\|v_i - v_j\|}{\sum_{i \ne j\,:\,x_i, x_j \in D_l}\|v_i - v_j\|} \\ &= \frac{1}{\sum_{i \ne j\,:\,x_i, x_j \in D_l}\|v_i - v_j\|} \sum_{i \ne j\,:\,x_i, x_j \in D_l} \frac{2n\,|D_l|}{c_B\,n_l\,(n_l - 1)} = \frac{2n\,|D_l|}{c_B\,\sum_{i \ne j\,:\,x_i, x_j \in D_l}\|v_i - v_j\|} \\ &= \hat{\pi}^{-1}\,. \end{aligned}$$

Thus, the time counter (3.4) has the correct expectation (2.22).

Note that in this procedure the rejections replace what we call fictitious jumps elsewhere.

Remark 3.3 *If, by chance, a pair* (i, j) *with a small relative velocity is chosen, then the time step (3.4) is large. This effect may create strong statistical fluctuations.*

3.3. Bird's "no time counter"

One chooses (cf. (2.21))

$$\hat{B}(v_i, v_j) = c_B \, U_{max} \tag{3.5}$$

where

$$U_{max} = U_{max}(\bar{z}) = \max_{i,j} \|v_i - v_j\| \, . \tag{3.6}$$

From (2.16) one obtains the time step

$$\hat{\tau}(\bar{z}) = \hat{\pi}(\bar{z})^{-1} = \frac{2\,n\,|D_l|}{c_B \, n_l \, (n_l - 1) \, U_{max}} \, . \tag{3.7}$$

The indices i, j are generated uniformly according to (2.17). The probability (2.18) of a fictitious jump is

$$1 - \frac{\|v_i - v_j\|}{U_{max}} \, . \tag{3.8}$$

The distribution of e is (2.24).

The value of $U_{max}(\bar{z})$ may change after each collision. Its calculation takes a quadratic effort with respect to n_l. Therefore, the following approximate procedure is used.

Let σ_k, $k = 1, 2, \ldots$, denote the time moments at which a (possibly fictitious) collision takes place, and i_k, j_k the corresponding indices of collision partners. Then the **accumulated maximal norm of the relative velocities** of collision partners up to the moment σ_k, i.e.

$$\tilde{U}_{max} = \tilde{U}_{max}(\sigma_k) = \max \left(\tilde{U}_{max}(0), \max_{l \le k} \|v_{i_l} - v_{j_l}\| \right) \, , \tag{3.9}$$

is used in (3.7) and (3.8) instead of U_{max} from (3.6).

Remark 3.4 *Since the function $\hat{B}(v_i, v_j) = c_B \, \tilde{U}_{max}$ does not usually satisfy (2.21) at the beginning of the collision simulation step, there will be a certain additional error in this procedure. This error will vanish when $\tilde{U}_{max}$ increases and adapts to the system. On the other hand, $\tilde{U}_{max}$ remembers all events from the past. Therefore it will be too large later on and create redundant fictitious collisions. These effects will be illustrated by numerical examples.*

3.4. Global bounds for the relative velocity norm

In the cell D_l we consider the **local mean velocity**

$$V = V(\bar{z}) = \frac{1}{n_l(\bar{z})} \sum_{i \, : \, x_i \in D_l} v_i \tag{3.10}$$

and the **local temperature**

$$T = T(\bar{z}) = \frac{1}{3\,n_l(\bar{z})} \sum_{i\,:\,x_i \in D_l} \|v_i - V(\bar{z})\|^2 = \frac{1}{3}\left[\frac{1}{n_l(\bar{z})} \sum_{i\,:\,x_i \in D_l} \|v_i\|^2 - \|V(\bar{z})\|^2\right]. \quad (3.11)$$

These quantities are preserved during the collision simulation step.

From the obvious inequalities

$$\|v_i - v_j\| \le 2 \max_i \|v_i - V(\bar{z})\|$$

and

$$\|v_i - V(\bar{z})\| = \left\| \frac{1}{n_l} \sum_{j=1}^{n_l} (v_i - v_j) \right\| \le \max_{i,j} \|v_i - v_j\|$$

one obtains

$$\max_i \|v_i - V(\bar{z})\| \le U_{max}(\bar{z}) \le 2 \max_i \|v_i - V(\bar{z})\|\,, \quad (3.12)$$

where U_{max} is defined in (3.6). The estimate (3.12) shows that the function

$$\hat{B}(v_i, v_j) = c_B\, \hat{U}_{max}\,, \quad (3.13)$$

where

$$\hat{U}_{max} = \hat{U}_{max}(\bar{z}) = 2 \max_i \|v_i - V(\bar{z})\|\,, \quad (3.14)$$

satisfies (2.21). By analogy with (3.5), U_{max} is to be replaced by $\hat{U}_{max}$ in (3.7) and (3.8). Thus, the time step is

$$\hat{\tau}(\bar{z}) = \hat{\pi}(\bar{z})^{-1} = \frac{2\,n\,|D_l|}{c_B\, n_l\,(n_l - 1)\,\hat{U}_{max}}\,. \quad (3.15)$$

The indices i, j are generated uniformly according to (2.17). The probability of a fictitious jump is

$$1 - \frac{\|v_i - v_j\|}{\hat{U}_{max}}\,. \quad (3.16)$$

The distribution of e is (2.24).

Remark 3.5 *The calculation of $\hat{U}_{max}(\bar{z})$ only takes linear effort in n_l. Numerical tests with this slight modification of the DSMC method will be presented.*

3.5. Localized upper bounds for the relative velocity norm

The definitions of the local mean velocity (3.10) and the local temperature (3.11) immediately imply that

$$\frac{1}{n_l} \sum_{i\,:\,x_i \in D_l} \frac{v_i - V(\bar{z})}{\sqrt{T(\bar{z})}} = 0 \quad \text{and} \quad \frac{1}{3\,n_l} \sum_{i\,:\,x_i \in D_l} \left\| \frac{v_i - V(\bar{z})}{\sqrt{T(\bar{z})}} \right\|^2 = 1\,.$$

It will be convenient to deal with the correspondingly normalized velocities in the cell D_l.

Consider some values

$$0 < b_1 < \ldots < b_K\,, \qquad K \geq 1\,, \tag{3.17}$$

where

$$\frac{\|v_i - V\|}{\sqrt{T}} \leq b_K\,, \quad \forall i\,. \tag{3.18}$$

Define

$$\hat{b}(v_i) = \min\left\{b_k\,,\ k = 1, \ldots, K : \frac{\|v_i - V\|}{\sqrt{T}} \leq b_k\right\}$$

and note that

$$\frac{\|v_i - V\|}{\sqrt{T}} \leq \hat{b}(v_i)\,, \quad \forall i\,. \tag{3.19}$$

The function $\hat{b}$ taking values $b_1, \ldots, b_K$ provides a certain non-global majorant for the normalized velocities. From (3.19) one obtains

$$\|v_i - v_j\| \leq \sqrt{T}\left[\frac{\|v_i - V\|}{\sqrt{T}} + \frac{\|v_j - V\|}{\sqrt{T}}\right] \leq \sqrt{T}\left[\hat{b}(v_i) + \hat{b}(v_j)\right].$$

Thus, the function

$$\hat{B}(v_i, v_j) = c_B\,\sqrt{T}\left[\hat{b}(v_i) + \hat{b}(v_j)\right] \tag{3.20}$$

satisfies (2.21).

The normalized velocities are divided into groups according to their individual majorants. Let

$$I_k = \{i\,:\,\hat{b}(v_i) = b_k\} \quad \text{and} \quad \gamma_k = \#I_k\,, \qquad k = 1, \ldots, K\,, \tag{3.21}$$

so that γ_k is the number of normalized velocities with the individual majorant b_k. We obtain from (2.16) and (3.20)

$$\begin{aligned}\hat{\pi}(\bar{z}) &= \frac{1}{2\,n\,|D_l|}\sum_{i\neq j\,:\,x_i, x_j \in D_l} c_B\,\sqrt{T}\left[\hat{b}(v_i) + \hat{b}(v_j)\right] \\ &= \frac{c_B\,\sqrt{T}\,2\,(n_l - 1)}{2\,n\,|D_l|}\sum_{i\,:\,x_i \in D_l}\hat{b}(v_i) = \frac{c_B\,\sqrt{T}\,2\,(n_l - 1)}{2\,n\,|D_l|}\sum_{k=1}^{K} b_k\,\gamma_k\,.\end{aligned}$$

The **time step** is

$$\hat{\tau}(\bar{z}) = \hat{\pi}(\bar{z})^{-1} = \frac{2\,n\,|D_l|}{c_B\,(n_l - 1)\,2\,\sqrt{T}\sum_{k=1}^{K} b_k\,\gamma_k}\,. \tag{3.22}$$

According to (2.17), (3.20), the **distribution of the indices** i and j takes the form

$$\frac{\hat{b}(v_i)+\hat{b}(v_j)}{2\,(n_l-1)\sum_{k=1}^{K} b_k\,\gamma_k} = \frac{1}{2}\,\frac{\hat{b}(v_i)}{(n_l-1)\sum_{k=1}^{K} b_k\,\gamma_k} + \frac{1}{2}\,\frac{\hat{b}(v_j)}{(n_l-1)\sum_{k=1}^{K} b_k\,\gamma_k}\,.$$

This means that one of the indices is distributed (on the set $\{i : x_i \in D_l\}$) according to the probabilities

$$\frac{\hat{b}(v_i)}{\sum_{k=1}^{K} b_k\,\gamma_k}\,,$$

the other is distributed uniformly. The order should be chosen with equal probability $\frac{1}{2}$. This last step can be omitted since the result of the jump does not depend on the order. Finally, we obtain a very simple procedure:

- choose the index of a group k on $\{1,\ldots,K\}$ according to the distribution

$$\frac{b_1\,\gamma_1}{\sum_{\mu=1}^{K} b_\mu\,\gamma_\mu},\ldots,\frac{b_K\,\gamma_K}{\sum_{\mu=1}^{K} b_\mu\,\gamma_\mu}\,; \tag{3.23}$$

- choose the index i of the first collision partner uniformly among the indices in the group I_k;
- choose the index j of the second collision partner uniformly on $\{j \neq i : x_j \in D_l\}$.

The **probability of a fictitious jump** is, according to (2.18), (2.20), (3.20),

$$1-\frac{\|v_i-v_j\|}{\sqrt{T}\left[\hat{b}(v_i)+\hat{b}(v_j)\right]}\,. \tag{3.24}$$

The distribution of e is (2.24).

Remark 3.6 *This modification of the DSMC method is expected to be more efficient than the standard method if there are relatively few particles with large relative velocity while the majority of particles has moderate relative velocities. In these cases the individual majorant (3.20) will be significantly better than the global majorant (3.13). This effect will be illustrated by numerical examples.*

Remark 3.7 *In our test calculations we define b_K from the initial configuration of the system as (cf. (3.18))*

$$b_K = \max\left\{\frac{\|v_i-V\|}{\sqrt{T}} \;:\; i=1,\ldots,n\,,\; x_i \in D_l\right\}, \tag{3.25}$$

and put

$$b_k = k\,\frac{b_K}{K}\,,\quad k=1,\ldots,K\,. \tag{3.26}$$

The value of b_K is increased (if necessary) during the simulation.

Remark 3.8 *The values of γ_k have to be updated after each collision. If some γ_k equals zero, then the corresponding group is simply not chosen (cf. (3.23)).*

4. Numerical experiments

4.1. Test example

The initial distribution of our test example is a weighted mixture of two Maxwellians, namely

$$f_0(v) = \alpha \frac{1}{(2\pi T_1)^{3/2}} \exp\left(-\frac{\|v - V_1\|^2}{2T_1}\right) + (1-\alpha)\frac{1}{(2\pi T_2)^{3/2}} \exp\left(-\frac{\|v - V_2\|^2}{2T_2}\right), \quad (4.1)$$

with

$$\alpha = 0.001\,, \quad V_1 = (-999, 0, 0)\,, \quad V_2 = (1, 0, 0)\,, \quad T_1 = 1\,, \quad T_2 = 1\,.$$

We consider the problem of calculating the time evolution of the second moments

$$m_{i,j}(t) = \int_{\mathcal{R}^3} v_i v_j f(t, v)\, dv\,, \quad i, j = 1, 2, 3\,, \quad (4.2)$$

and the third moments

$$r_i(t) = \int_{\mathcal{R}^3} v_i \|v\|^2 f(t, v)\, dv\,, \quad i = 1, 2, 3\,. \quad (4.3)$$

The function $f(t, v)$ is the solution of the spatially homogeneous Boltzmann equation with the initial condition $f(0, v) = f_0(v)$. In addition, we calculate some shell-functionals, which are of the form

$$S_{[a,b]}(t) = \int_{\mathcal{R}^3} \varphi(v, V, T) f(t, v)\, dv\,, \quad (4.4)$$

where

$$\varphi(v, V, T) = \begin{cases} 1\,, & \text{if } \frac{\|v-V\|}{\sqrt{T}} \in [a, b)\,, \\ 0\,, & \text{otherwise}\,. \end{cases}$$

A particle system approximating the distribution (4.1) consists of many particles ($\sim$ 99.9%) with small velocities ($\sim V_2$) and of a few particles ($\sim$ 0.1%) with large velocities ($\sim V_1$). The system relaxes to a Maxwellian with mean velocity $\bar{V} = 0$ and temperature $\bar{T} = 334$.

We apply three methods:

- the standard DSMC method with the accumulated maximal norm of the relative velocities (described in § 3.3);
- the modification of the DSMC method with the adaptive global upper bound for the norm of the relative velocities (described in § 3.4);
- the modification of the DSMC method with the localized upper bound for the norm of the relative velocities (described in § 3.5).

4.2. Statistical notions

First we introduce some definitions and notations that are helpful for the understanding of stochastic numerical procedures.

Functionals of the form

$$F(t) = \int_{\mathcal{R}^3} \varphi(v)\, f(t,v)\, dv\,. \tag{4.5}$$

are approximated by the random variable

$$\xi^{(n)}(t) = \frac{1}{n}\sum_{i=1}^{n} \varphi(v_i(t))\,, \tag{4.6}$$

where $(v_1(t),\ldots,v_n(t))$ is the particle system. In order to estimate and to reduce the random fluctuations of the estimator (4.6), a number N of independent ensembles of particles is generated. The corresponding values of the random variable are denoted by

$$\xi_1^{(n)}(t),\ldots,\xi_N^{(n)}(t)\,.$$

The **empirical mean value** of the random variable (4.6)

$$\eta_1^{(n,N)}(t) = \frac{1}{N}\sum_{j=1}^{N} \xi_j^{(n)}(t) \tag{4.7}$$

is then used as an approximation to the functional (4.5). The error of this approximation is

$$e^{(n,N)}(t) = |\eta_1^{(n,N)}(t) - F(t)|$$

and consists of the following two components.

The **systematic error** is the difference between the mathematical expectation of the random variable (4.6) and the exact value of the functional, i.e.

$$e_{sys}^{(n)}(t) = E\xi^{(n)}(t) - F(t)\,.$$

The **statistical error** is the difference between the empirical mean value and the expected value of the random variable, i.e.

$$e_{stat}^{(n,N)}(t) = \eta_1^{(n,N)}(t) - E\xi^{(n)}(t)\,.$$

A **confidence interval** for the expectation of the random variable $\xi^{(n)}(t)$ is obtained as

$$I_p = \left[\eta_1^{(n,N)}(t) - \lambda_p\sqrt{\frac{\operatorname{Var}\xi^{(n)}(t)}{N}}\,,\ \eta_1^{(n,N)}(t) + \lambda_p\sqrt{\frac{\operatorname{Var}\xi^{(n)}(t)}{N}}\right], \tag{4.8}$$

where

$$\operatorname{Var}\xi^{(n)}(t) := E\left[\xi^{(n)}(t) - E\xi^{(n)}(t)\right]^2 = E\left[\xi^{(n)}(t)\right]^2 - \left[E\xi^{(n)}(t)\right]^2 \tag{4.9}$$

is the **variance** of the random variable (4.6), and $p \in (0,1)$ is the **confidence level**. This means that

$$\text{Prob}\left\{E\xi^{(n)}(t) \notin I_p\right\} = \text{Prob}\left\{|e_{stat}^{(n,N)}(t)| \geq \lambda_p \sqrt{\frac{\text{Var}\,\xi^{(n)}(t)}{N}}\right\} \sim p\,.$$

Thus, the value

$$c^{(n,N)}(t) = \lambda_p \sqrt{\frac{\text{Var}\,\xi^{(n)}(t)}{N}} \tag{4.10}$$

is a probabilistic upper bound for the statistical error.

In the calculations we use a confidence level of $p = 0.999$ and $\lambda_p = 3.2$. The variance is approximated by the corresponding empirical value (cf. (4.9)), i.e.

$$\text{Var}\,\xi^{(n)}(t) \sim \eta_2^{(n,N)}(t) - \left[\eta_1^{(n,N)}(t)\right]^2,$$

where

$$\eta_2^{(n,N)}(t) = \frac{1}{N}\sum_{j=1}^{N}\left[\xi_j^{(n)}(t)\right]^2$$

is the **empirical second moment** of the random variable (4.6).

4.3. Influence of the relative velocity bounds

First we study the relationship between the accumulated maximal norm of the relative velocities $\tilde{U}_{max}$ (cf. (3.9)) and the adaptive upper bound for the norm of the relative velocities $\hat{U}_{max}$ (cf. (3.14)). The behaviour of these quantities is displayed in **Figure 1** on different time intervals and for different particle numbers. The thick lines represent $\tilde{U}_{max}$, while the two thin lines represent the lower and upper bounds in (3.12) (the upper bound being $\hat{U}_{max}$). On longer time intervals, the difference between $\tilde{U}_{max}$ and $\hat{U}_{max}$ becomes quite significant. In the starting interval, where $\tilde{U}_{max}$ is less than the lower bound in (3.12), a certain additional systematic error is expected for the method from § 3.3. However, this interval becomes smaller when the number of particles increases.

Next we study the influence of different relative velocity bounds on various numbers of collisions. **Figure 2** shows the behaviour of real and fictitious collisions for different methods and the particle number $n = 100000$. The numbers of real collisions are (as they should be) almost identical. The numbers of fictitious collisions are quite different. The lines (from above) correspond to the methods from § 3.3, § 3.4, and § 3.5 (with $K = 16$ and $K = 64$ in (3.25), (3.26)).

More detailed information is contained in **Tables 1** and **2**. The last but one columns in these tables show the number of collisions for different methods in relation to the standard DSMC method. The last columns show the corresponding relative values for the CPU time. Table 2 shows, for example, that the method from § 3.4 needs only half of the collisions compared with the standard method. However, this advantage is cancelled out by the additional effort needed for updating the bound for the norm of the relative

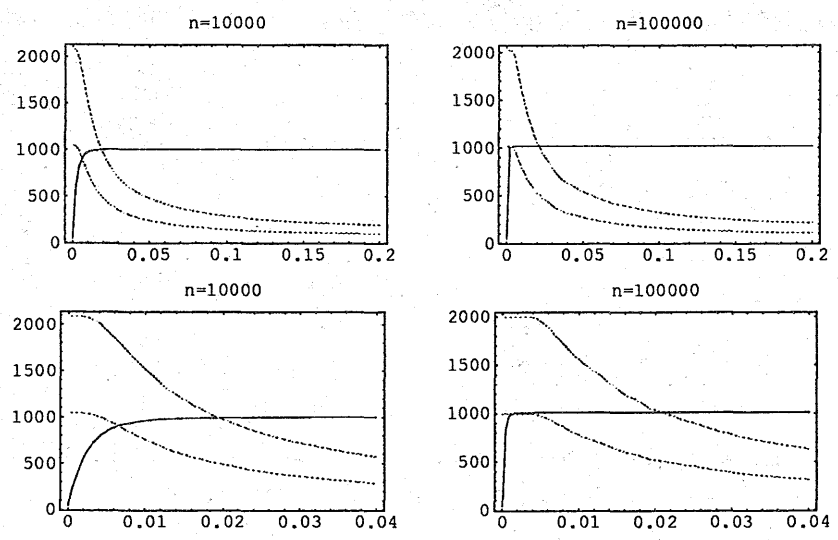

Figure 1: Relative velocity bounds

velocities. The method from § 3.5 with $K = 64$ gives a gain factor of about 16 as far as the number of collisions is concerned. Most of this advantage is lost due to the effort needed for sorting the particles with respect to the local bounds. However, a gain factor of 2 remains. This factor becomes larger on longer time intervals.

Table 1

time	n	N	method	real	fict. (%)	coll	CPU
0.04	100000	100	§ 3.3	32069	98.4	1.00	1.00
0.04	100000	100	§ 3.4	32377	98.6	1.15	1.10
0.04	100000	100	§ 3.5/K=4	32361	96.8	0.50	0.94
0.04	100000	100	§ 3.5/K=8	32159	93.7	0.25	0.85
0.04	100000	100	§ 3.5/K=64	32504	63.6	0.05	0.80

Table 2

time	n	N	method	real	fict. (%)	coll	CPU
0.2	100000	100	§ 3.3	330123	96.8	1.00	1.00
0.2	100000	100	§ 3.4	333054	93.3	0.48	1.00
0.2	100000	100	§ 3.5/K=4	334633	93.3	0.48	0.82
0.2	100000	100	§ 3.5/K=16	332348	74.7	0.13	0.52
0.2	100000	100	§ 3.5/K=64	338708	46.7	0.06	0.48
0.2	100000	100	§ 3.5/K=256	336520	28.9	0.05	1.31

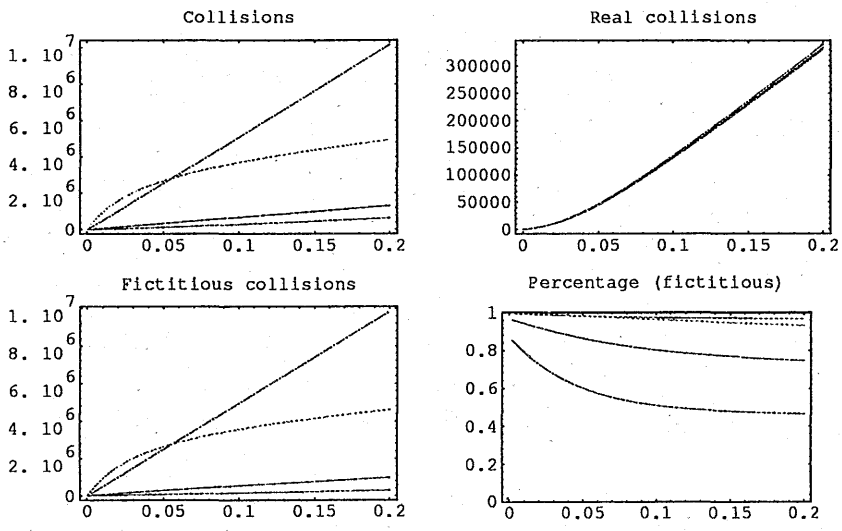

Figure 2: Numbers of collisions for different methods

4.4. Relaxation of moments

Here we study the behaviour of the moments (4.2), (4.3) as $t \to \infty$, and the dependence of this behaviour on the number of particles.

Figure 3 shows the dependence on n of the time evolution of the functional $r_1(t)$ calculated with the standard DSMC method from § 3.3. The systematic error is due to the deviation of $\tilde{U}_{max}$ from U_{max}, which was investigated in the previous section. For small n, the time steps are too large at the beginning. Thus, increasing curves are moved to the right. The confidence intervals are displayed according to (4.8). The curve for $n = 100000$ is correct and identical to the curves for all other methods with $n = 1000, 10000, 100000$.

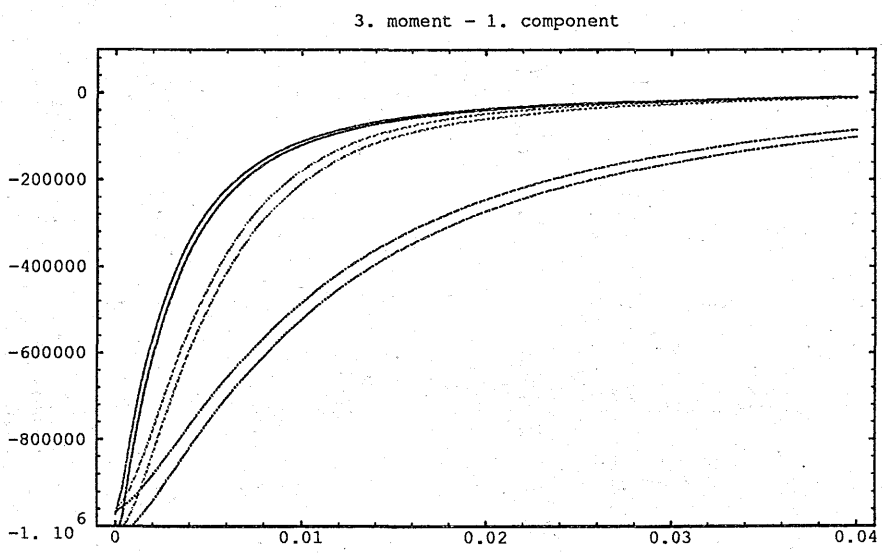

Figure 3: Method from § 3.3 with $n = 1000, 10000, 100000$ (from below)

Now we consider the particle number $n = 100000$, where the results for different methods are identical. The time evolution of all moments (4.2), (4.3) is displayed in **Figure 4** on a small time interval. At the end of the time interval the exact stationary values are already in the confidence interval, except for the first component of the third moment $r_1(t)$. Here the detailed picture shows that this is not yet the case. **Figures 5** and **6** show the corresponding behaviour on a medium and a long time interval. Note that only at a time of about 0.3 the functional $r_1(t)$ reaches its exact stationary value.

More details are contained in **Tables 3-5**. The values of the estimates (4.7) and the corresponding statistical error bounds (4.10) are provided for the functional $r_1(t)$ (cf. (4.3)) for different methods, time intervals, and particle numbers. In addition to what has been already pointed out in connection with Figures 4-6, Table 5 shows that there is still a systematic error in the stationary values for n=1000 and n=10000. The exact value is only inside the confidence interval for n=100000.

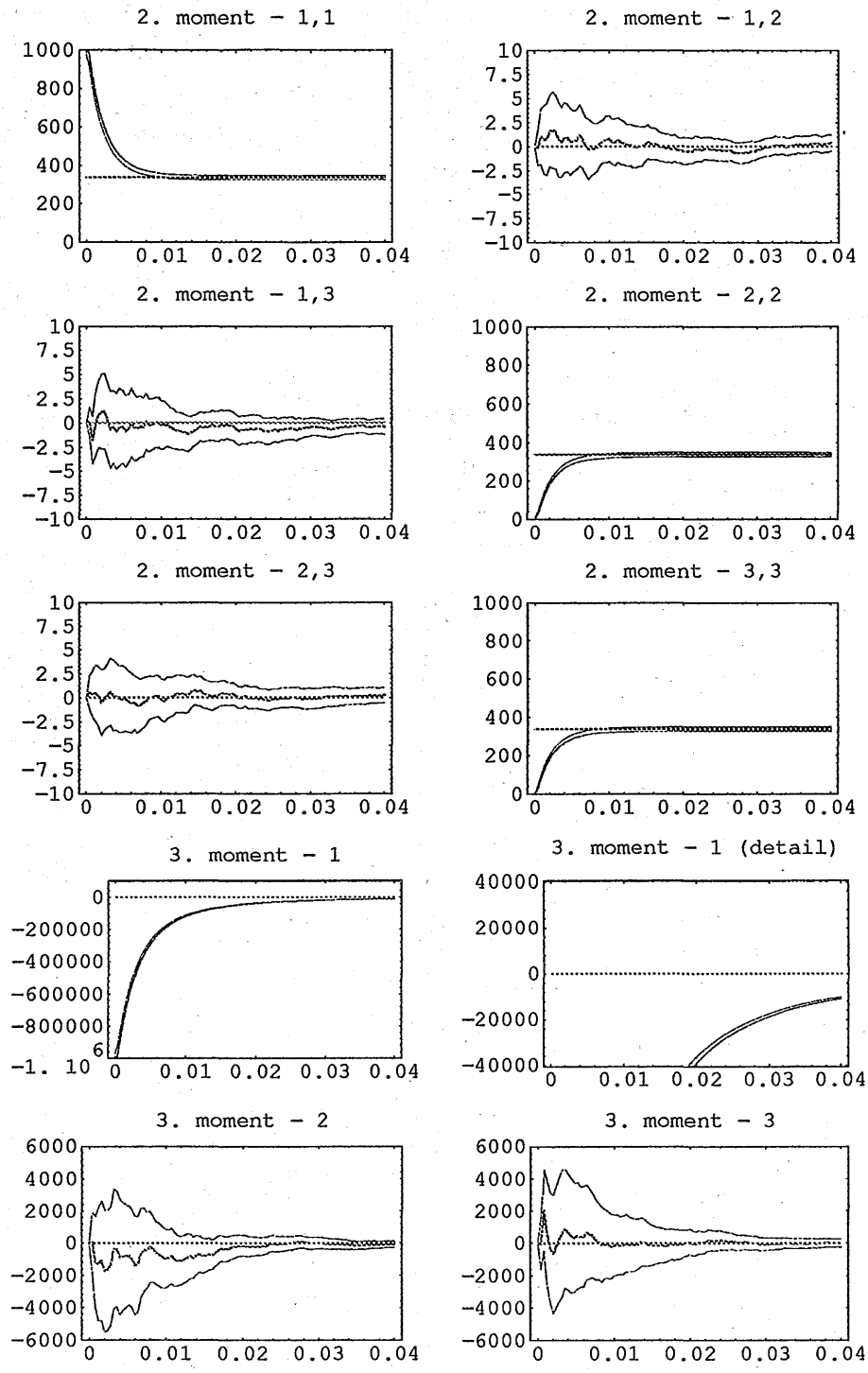

Figure 4: Moments on a short time interval

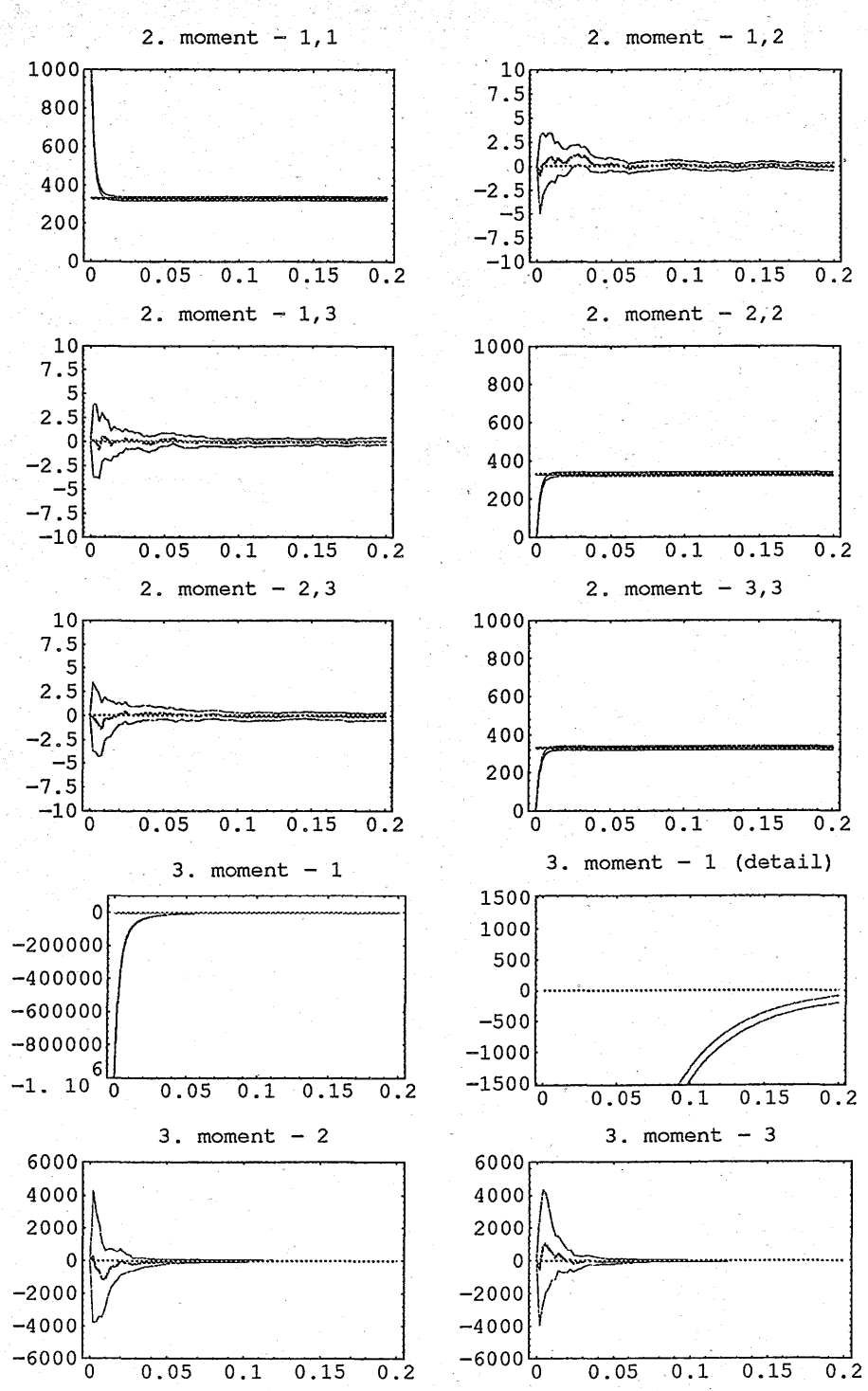

Figure 5: Moments on a medium time interval

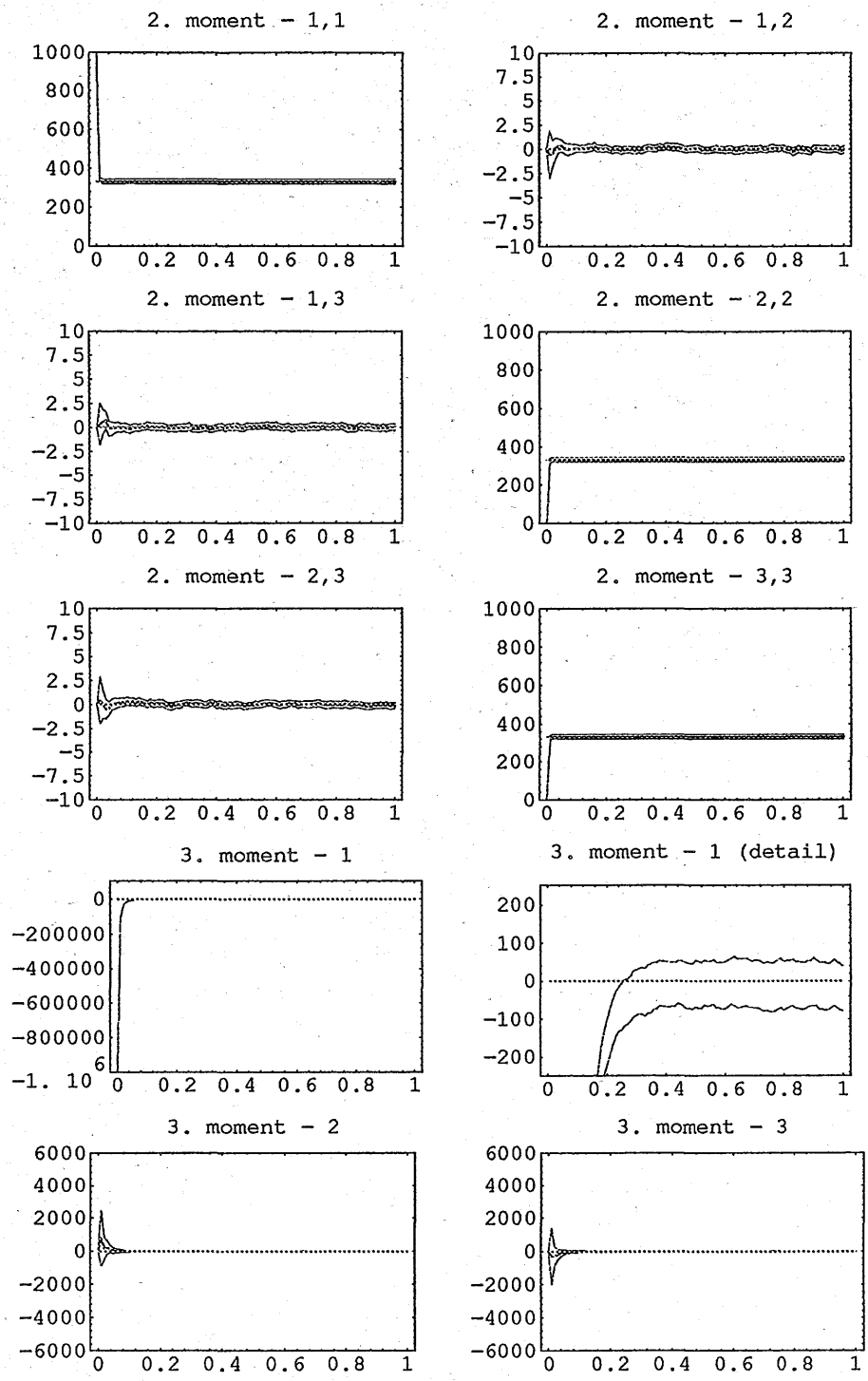

Figure 6: Moments on a long time interval

Table 3

t	n	N	method	$r_1^{(n)}(0), r_1^{(n)}(t/2), r_1^{(n)}(t)$	conf. bounds
0.04	1000	10000	§ 3.3	-999224, -265069, -93721	32471, 13807, 8195
0.04	1000	10000	§ 3.4	-1002827, -38731, -11339	31986, 1494, 455
0.04	1000	10000	§ 3.5/K=4	-998123, -38772, -11332	31454, 1458, 458
0.04	1000	10000	§ 3.5/K=8	-1002008, -38971, -11341	32279, 1504, 469
0.04	1000	10000	§ 3.5/K=64	-991583, -38382, -11162	31672, 1475, 457
0.04	10000	1000	§ 3.3	-992973, -55523, -12096	31198, 6022, 789
0.04	10000	1000	§ 3.4	-1007682, -38474, -10422	32385, 1483, 445
0.04	10000	1000	§ 3.5/K=4	-1005091, -38431, -10224	30879, 1446, 406
0.04	10000	1000	§ 3.5/K=8	-1003321, -37871, -10461	30828, 1441, 419
0.04	10000	1000	§ 3.5/K=64	-993212, -37593, -10216	30719, 1397, 408
0.04	100000	100	§ 3.3	-1005132, -39108, -10460	32647, 1394, 394
0.04	100000	100	§ 3.4	-1005382, -38344, -10260	33376, 1462, 446
0.04	100000	100	§ 3.5/K=4	-1006211, -38220, -10234	32276, 1481, 446
0.04	100000	100	§ 3.5/K=8	-995805, -37671, -10125	29834, 1291, 401
0.04	100000	100	§ 3.5/K=64	-1010693, -38387, -10291	33515, 1446, 422

Table 4

t	n	N	method	$r_1^{(n)}(0), r_1^{(n)}(t/2), r_1^{(n)}(t)$	conf. bounds
0.2	10000	1000	§ 3.3	-998392, -1670, -316	30624, 104, 68
0.2	10000	1000	§ 3.4	-994193, -1549, -307	32003, 104, 67
0.2	10000	1000	§ 3.5/K=64	-993032, -1585, -317	31313, 103, 66
0.2	100000	100	§ 3.3	-983604, -1431, -148	30991, 101, 58
0.2	100000	100	§ 3.4	-995456, -1501, -178	34683, 114, 63
0.2	100000	100	§ 3.5/K=4	-1002561, -1487, -186	32766, 105, 61
0.2	100000	100	§ 3.5/K=16	-991378, -1439, -157	30813, 102, 62
0.2	100000	100	§ 3.5/K=64	-1022255, -1538, -217	30124, 99, 55
0.2	100000	100	§ 3.5/K=256	-1011767, -1489, -207	29479, 94, 54

Table 5

t	n	N	method	$r_1^{(n)}(0), r_1^{(n)}(t/2), r_1^{(n)}(t)$	conf. bounds
1.0	1000	10000	§ 3.5/K=64	-988719, -1677, -1665	32088, 143, 141
1.0	10000	1000	§ 3.4	-1010812, -188, -189	31942, 70, 70
1.0	10000	1000	§ 3.5/K=64	-987763, -153, -156	32014, 66, 68
1.0	100000	100	§ 3.4	-994765, -13, -17	34622, 60, 63
1.0	100000	100	§ 3.5/K=4	-1010652, -48, -49	32017, 59, 59
1.0	100000	100	§ 3.5/K=64	-991310, -13, -19	34112, 60, 58

4.5. Relaxation of shell functionals

Here we calculate the time evolution of functionals of the form (4.4). The behaviour of these functionals illustrates the phenomenon of relaxation rather impressively. We consider the particle number $n = 100000$, and use the method from § 3.5. The other methods give the same results but are slower.

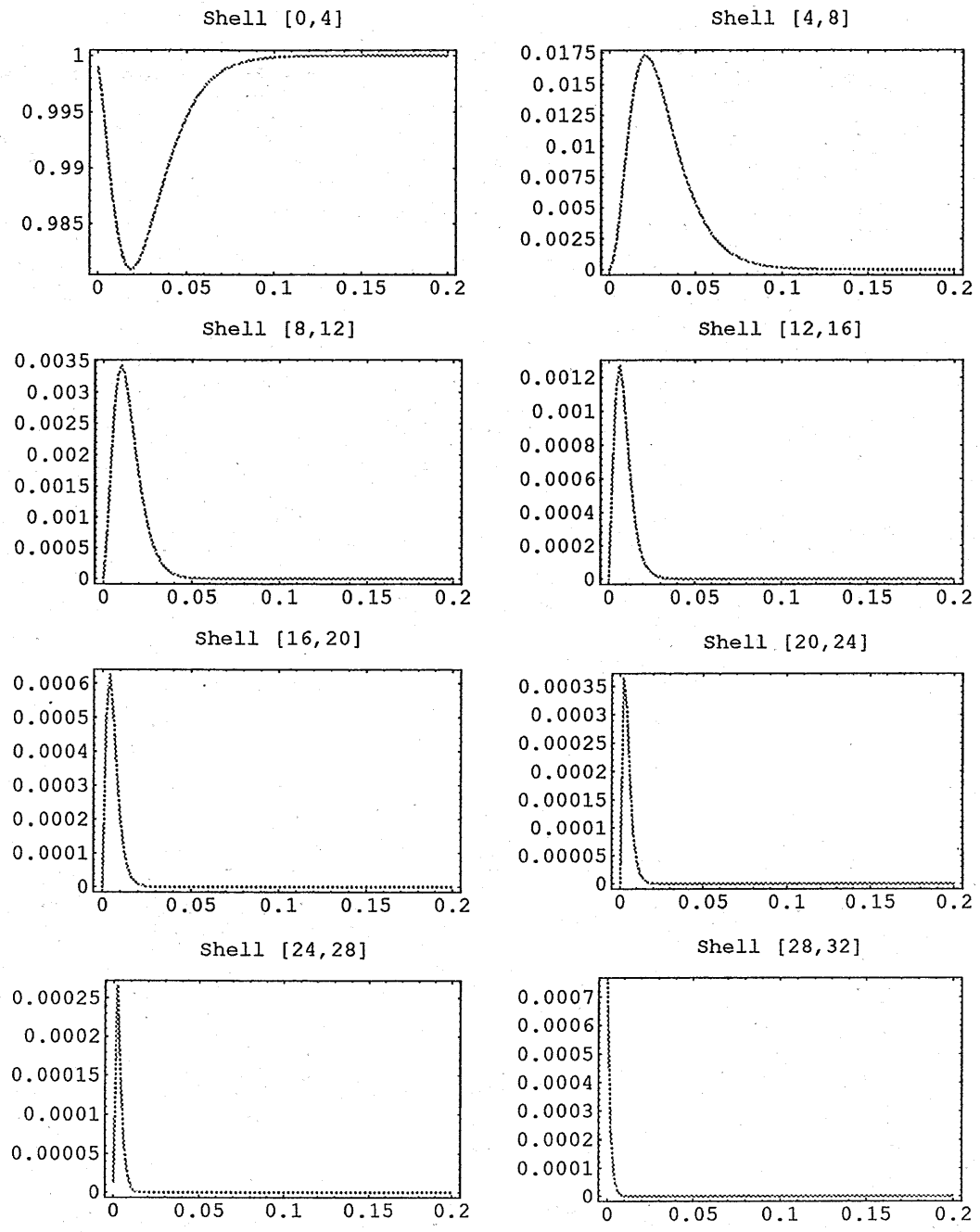

Figure 7: Large shells on a medium time interval

Figure 7 shows how the small number of particles with large velocities relaxes to the inner shell $[0, 4]$.

Next we divide the inner shell into smaller subshells. **Figure 8** shows that the corresponding functionals have not yet relaxed. Relaxation of those functionals only takes place on the longer time interval in **Figure 9**. The constant lines represent the exact stationary values, which were calculated analytically.

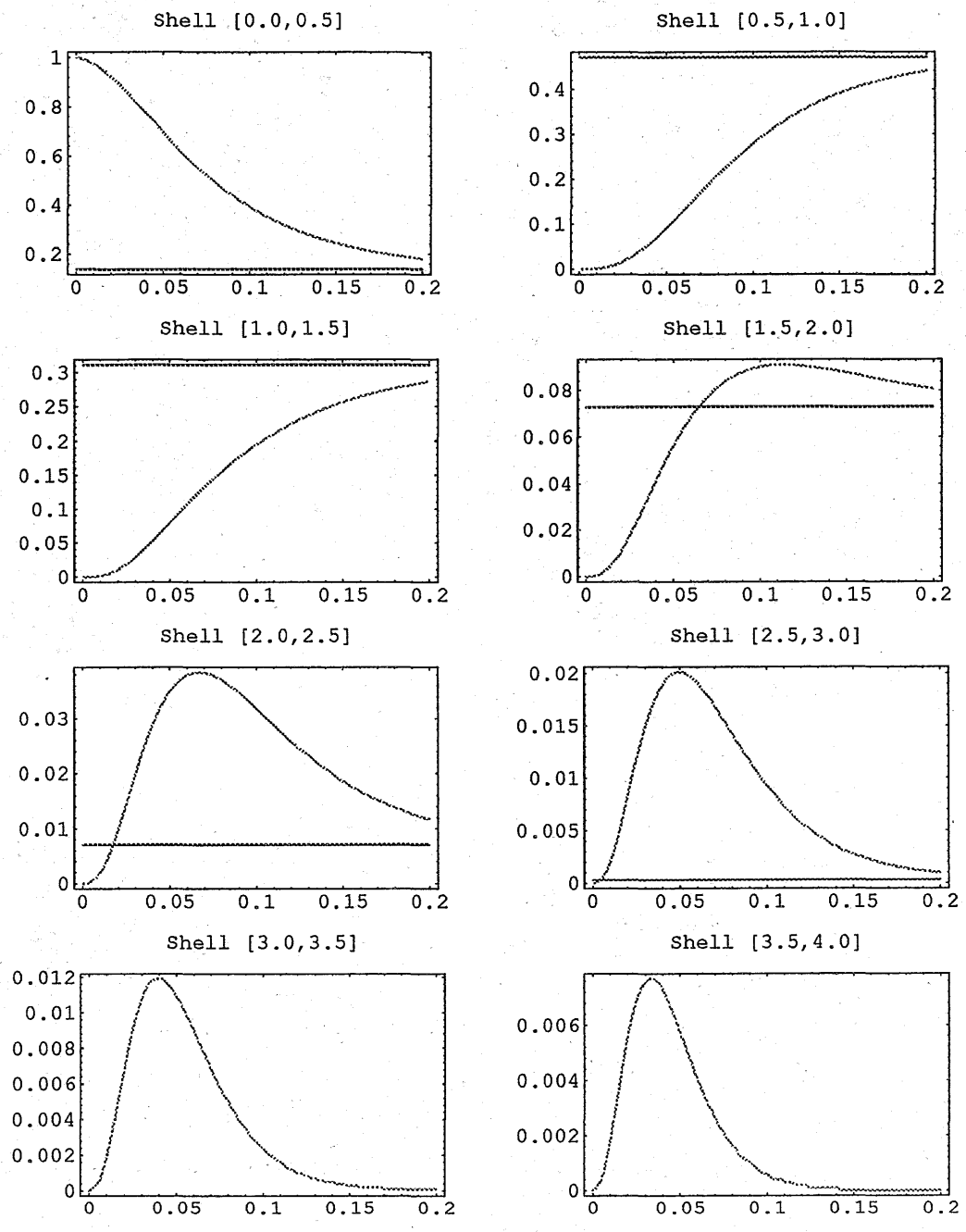

Figure 8: Small shells on a medium time interval

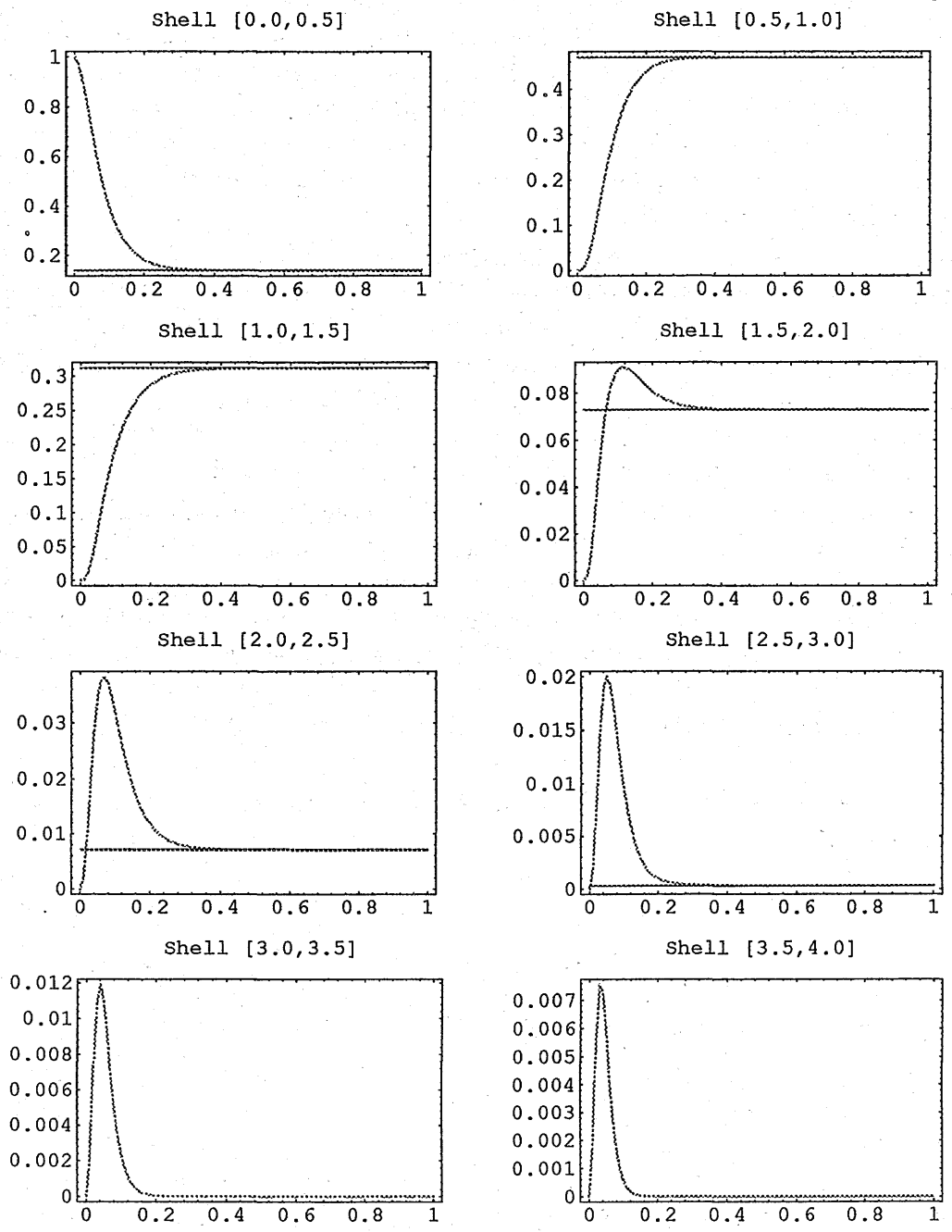

Figure 9: Small shells on a long time interval

5. Conclusions

The algorithms studied in this paper contain three main components – the time steps, the distribution of the collision partners, and the probability of fictitious collisions. The first and third component are closely related to each other. If the time step is small then there are many attempts to collide and the probability of fictitious collisions must be large, since the number of real collisions should remain constant (see Figure 2). Thus, the average size of the time step is well represented by the number of all (real and fictitious) collisions (see Tables 1 and 2).

There is an interplay between the time steps and the distribution of the collision partners. In the standard DSMC scheme from § 3.3 there are small time steps, but a very simple distribution of the collision partners. In the modification from § 3.5 the time steps are much larger. However, more effort has to be spent in order to generate the distribution of the collision partners. In the modification from § 3.4 the time steps are larger than in the standard method and the distribution of the collision partners is the same. However, the calculation of the time steps is more expensive.

Using different modifications of the DSMC method, several effects were observed. Adaptive bounds for the norm of the relative velocities (as in the method of § 3.4) lead to a reduction of the systematic error, since they avoid the wrong time scale at the beginning of the relaxation period (see Figure 3). Localized bounds for the norm of the relative velocities (as in the method of § 3.5) lead to a significant reduction of the number of fictitious collisions. Of course, the particular initial distribution (4.1) was chosen to illustrate the inefficiency of the standard DSMC method with the accumulated maximal relative velocity norm in certain situations.

Several other modifications of the DSMC method seem to be of interest. For example, an adaptive value of b_K (cf. (3.25)) in the method of § 3.5 can be considered. Comparing the time step (3.22) with (3.15) one notes that the factor $n_l \hat{U}_{max}$ is replaced by $2\sqrt{T}\sum_{k=1}^{K} b_k \gamma_k$. Taking into account (3.17), (3.21), (3.25), and (3.14), one obtains that

$$2\sqrt{T}\sum_{k=1}^{K} b_k \gamma_k \leq 2\sqrt{T}\, b_K \sum_{k=1}^{K} \gamma_k = 2\sqrt{T}\, b_K\, n_l = \hat{U}_{max}\, n_l\,.$$

Thus the time step (3.22) is always larger than the time step (3.15) of the standard DSMC method with the adaptive bound for the relative velocity norm. In the case $K = 1$, one obtains $2\, b_1 \sqrt{T} = \hat{U}_{max}$ and $\gamma_1 = n_l$. Thus, the time steps are equal. The indices i, j are distributed uniformly. The probabilities of a fictitious jump are also the same (cf. (3.16), (3.24)). Thus, the modification of the DSMC method from § 3.4 is a special case. Another opportunity is to derive a method with a constant time step containing the local temperature (3.11) instead of some bound for the relative velocity norm. This would avoid the corresponding systematic error and make the method more stable with respect to small perturbations of the flow. Work on these modifications is in progress.

The approach developed in this paper opens a field for further investigations on the DSMC method. New modifications can be derived adapting the method to special applications.

References

[1] G. A. Bird. Approach to translational equilibrium in a rigid sphere gas. *Phys. Fluids*, 6:1518–1519, 1963.

[2] G. A. Bird. Direct simulation and the Boltzmann equation. *Phys. Fluids*, 13(11):2676–2681, 1970.

[3] G. A. Bird. *Molecular Gas Dynamics.* Clarendon Press, Oxford, 1976.

[4] G. A. Bird. Perception of numerical methods in rarefied gas dynamics. *Progr. Astronaut. Aeronaut.*, 118:211–226, 1989.

[5] G. A. Bird. *Molecular Gas Dynamics and the Direct Simulation of Gas Flows.* Clarendon Press, Oxford, 1994.

[6] C. Cercignani. *The Boltzmann Equation and its Applications.* Springer, New York, 1988.

[7] C. Cercignani, R. Illner, and M. Pulvirenti. *The Mathematical Theory of Dilute Gases.* Springer, New York, 1994.

[8] K. Koura. Null–collision technique in the direct–simulation Monte Carlo method. *Phys. Fluids*, 29(11):3509–3511, 1986.

[9] *Rarefied Gas Dynamics (J. Harvey and G. Lord, eds.)*, volume 1 and 2, Oxford University Press, Oxford, 1995.

[10] S. Rjasanow and W. Wagner. A stochastic weighted particle method for the Boltzmann equation. *J. Comput. Phys.*, 124(2):243–253, 1996.

[11] W. Wagner. A convergence proof for Bird's direct simulation Monte Carlo method for the Boltzmann equation. *J. Statist. Phys.*, 66(3/4):1011–1044, 1992.

[12] W. Wagner. A stochastic particle system associated with the spatially inhomogeneous Boltzmann equation. *Transport Theory Statist. Phys.*, 23(4):455–477, 1994.

Recent publications of the Weierstraß–Institut für Angewandte Analysis und Stochastik

Preprints 1997

320. Sergej Rjasanow, Thomas Schreiber, Wolfgang Wagner: Reduction of the number of particles in the stochastic weighted particle method for the Boltzmann equation.

321. Wolfgang Dahmen, Angela Kunoth, Karsten Urban: Wavelets in numerical analysis and their quantitative properties.

322. Michael V. Tretyakov: Numerical studies of stochastic resonance.

323. Johannes Elschner, Gunther Schmidt: Analysis and numerics for the optimal design of binary diffractive gratings.

324. Ion Grama, Michael Nussbaum: A nonstandard Hungarian construction for partial sums.

325. Siegfried Prössdorf, Jörg Schult: Multiwavelet approximation methods for pseudodifferential equations on curves. Stability and convergence analysis.

326. Peter E. Kloeden, Alexander M. Krasnosel'skii: Twice degenerate equations in the spaces of vector-valued functions.

327. Nikolai A. Bobylev, Peter E. Kloeden: Periodic solutions of autonomous systems under discretization.

328. Martin Brokate Pavel Krejčí: Maximum Norm Wellposedness of Nonlinear Kinematic Hardening Models.

329. Ibrahim Saad Abdel-Fattah: Stability Analysis of Quadrature Methods for Two-Dimensional Singular Integral Equations.

330. Wolfgang Dreyer, Wolf Weiss: Geschichten der Thermodynamik und obskure Anwendungen des zweiten Hauptsatzes.

331. Klaus Fleischmann, Achim Klenke: Smooth density field of catalytic super-Brownian motion.

332. V. G. Spokoiny: Image denoising: Pointwise adaptive approach.

333. Jens. A. Griepentrog: An application of the Implicit Function Theorem to an energy model of the semiconductor theory.

334. Todd Kapitula, Björn Sandstede: Stability of bright solitary-wave solutions to perturbed nonlinear Schrödinger equations.

335. J. Sprekels, D. Tiba: A duality approach in the optimization of beams and plates.

336. R. Dobrushin, O. Hryniv: Fluctuations of the Phase Boundary in the $2D$ Ising Ferromagnet.

337. A. Bovier, V. Gayrard, P. Picco: Typical profiles of the Kac-Hopfield model.

338. Annegret Glitzky, Rolf Hünlich: Global estimates and asymptotics for electro-reaction-diffusion systems in heterostructures.

339. Hans-Christoph Kaiser, Joachim Rehberg[1]: About a stationary Schrödinger-Poisson system with Kohn-Sham potential in nanoelectronics.

340. Dan Tiba: Maximal monotonicity and convex programming.

341. Anton Bovier, Véronique Gayrard: Metastates in the Hopfield model in the replica symmetric regime.

342. Ilja Schmelzer: Generalization of Lorentz-Poincare ether theory to quantum gravity.

343. Gottfried Bruckner, Sybille Handrock-Meyer, Hartmut Langmach: An inverse problem from the 2D-groundwater modelling.

344. Pavel Krejčí, Jürgen Sprekels: Temperature-Dependent Hysteresis in One-Dimensional Thermovisco-Elastoplasticity.

345. Uwe Bandelow, Lutz Recke, Björn Sandstede: Frequency Regions for Forced Locking of Self-Pulsating Multi-Section DFB Lasers.

346. Peter E. Kloeden, Jerzy Ombach, Alexei V. Pokrovskii: Continuous and inverse shadowing.

347. Grigori N. Milstein: On the mean-square approximation of a diffusion process in a bounded domain.

348. Anton Bovier: The Kac Version of the Sherrington-Kirkpatrick Model at High Temperatures.